13. A lattice mismatch bigger than 0.1% between substrate and film is thought to cause pseudomorphic growth, which results in films with crystallographic defects (*11*). In addition, the difference in the thermal expansion coefficients between epilayer and substrate produces thermal stresses at the interface (*12*).
14. H. J. Osten, J. Klatt, G. Lippert, *Appl. Phys. Lett.* **60**, 44 (1992).
15. F. S. Ohuci, B. A. Parkinson, K Ueno, A. Koma, *J. Appl. Phys.* **68**, 2168 (1990).
16. S. W. Bailey, in *Review in Minerology Micas*, S. W. Bailey, Ed. (Mineralogical Society of America, Chelsea, MI, 1984), vol. 13, chap. 2, pp. 13–60.
17. B. G. Hyde and S. Anderson, *Inorganic Crystal Structures* (Wiley, New York, 1989).
18. Vacuum Generators, ESCALAB, Center for Materials Research, Stanford University, Stanford, CA.
19. M. P. Seah and W. A. Dench, *Surf. Interface Anal.* **1**, 2 (1979).
20. J. H. Scofield, *J. Electron Spectrosc. Relat. Phenom.* **8**, 129 (1976).
21. J. Olivier and R. Poirier, *Surf. Sci.* **105**, 347 (1981).
22. Nanoscope II FM, Digital Instruments, Inc., Goleta, CA.
23. Although both the shape of the scanning tip and the interaction between tip and sample may influence the finer details of a measured image [N. A. Burnham and R. J. Colton, in *Scanning Tunneling Microscopy: Theory and Application*, D. Bonnell, Ed. (VCH Publishers, New York, 1993), chap. 7, p. 240], it is clear that the surface is very smooth and crystalline. If the recorded amplitude of 0.2 nm were artificially amplified because of such tip-substrate interactions, this would indicate that the surfaces are even smoother than the value quoted.
24. Possible systematic errors due to the calibration in the *x* and *y* directions from images of mica (*30*) are not included.
25. The higher adhesion energy measured in air between surfaces that have been prepared by VDWE as compared to the values for VPD sapphire further attest to the angstrom-scale smoothness in the former case.
26. E. A. D. White and J. D. C. Wood, *J. Mater. Sci.* **9**, 1999 (1974).
27. J. N. Israelachvili, P. M. McGuiggan, A. M. Homola, *Science* **240**, 189 (1988).
28. Recent molecular dynamic simulations with flexible linear chains trapped between two [111] planes of a face-centered-cubic lattice indicate a wall-induced glass transition of fluid films [P. A. Thompson, G. S. Grest, M. O. Robbins, *Phys. Rev. Lett.* **68**, 3448 (1992)].
29. M. L. Gee, P. M. McGuiggan, J. N. Israelachvili, *J. Chem. Phys.* **93**, 1845 (1990).
30. D. K. Schwartz, J. Garnaes, R. Viswanathan, J. A. N. Zasadzinski, *Science* **257**, 508 (1992).
31. Supported by Office of Naval Research (ONR) grant N00014-89-J-1101. We thank J. Zasadzinski for providing his AFM facility (supported by ONR grant N00014-90-J-1551) and D. Pearson, F. Lange, E. Hu, D. Schwartz, and M. Chaudhuri for helpful discussions.

30 November 1992; accepted 24 February 1993

Preparation of Amorphous Boron Nitride and Its Conversion to a Turbostratic, Tubular Form

Ewan J. M. Hamilton, Shawn E. Dolan, Charles M. Mann, Hendrik O. Colijn, Clare A. McDonald, Sheldon G. Shore*

Amorphous boron nitride, BN, is obtained from the reaction of *B*-trichloroborazine, $(BClNH)_3$, with cesium metal. The amorphous product is converted to a turbostratic form upon heating to 1100°C. Scanning electron microscopy reveals a previously unreported morphology composed of hollow tubular structures. The largest of these appear to be approximately 3 micrometers in external diameter and 50 to 100 micrometers in length. Transmission electron microscopy and selected-area electron diffraction also indicate the tube walls to be turbostratic in nature. The mechanism by which the tubes form is not known, although apparent sites of incipient tube growth have been observed.

When amorphous boron nitride (BN) obtained from the reaction between cesium and *B*-trichloroborazine ($B_3Cl_3N_3H_3$) is heated under vacuum to 1100°C, it is converted to two morphologies of turbostratic (*1*) boron nitride, a partially ordered, pseudographitic form. [A turbostratic phase of a layered material is characterized by rotational disorder in the direction normal to the layers (*1*).] In addition to the commonly observed distorted lamellar form, scanning electron microscopy (SEM) reveals the presence of hollow tubular structures, a previously unreported morphology for BN. These tubes form in a range of sizes, with diameters of approximately 3 μm and 0.15 μm being most commonly observed. High-resolution microscopy reveals that the tube walls do not possess a high degree of crystallinity but rather are turbostratic in nature.

E. J. M. Hamilton, S. E. Dolan, C. M. Mann, S. G. Shore, Department of Chemistry, Ohio State University, Columbus, OH 43210.
H. O. Colijn and C. A. McDonald, Department of Materials Science and Engineering, Ohio State University, Columbus, OH 43210.
*To whom correspondence should be addressed.

Although the mechanism of formation of this new morphology is unclear, it appears that our synthesis of the amorphous BN precursor may be a crucial factor. Traditionally, BN powders have been prepared by classical, high-temperature syntheses (*2*). These typically involve inexpensive boron- and nitrogen-bearing reagents, such as boric acid and ammonia, but complicated work-up procedures are required to obtain a product of high purity. We have developed a procedure for synthesizing amorphous BN that involves an explosive reaction between *B*-trichloroborazine and cesium metal initiated at 125°C in the absence of a solvent; HCl, H_2, and CsCl are also formed (*3*).

After removal of the by-products (*3*), x-ray powder diffraction patterns (*4*) and SEM images (*4*) reveal the amorphous nature of the BN product. Heating to 1100°C under vacuum for 24 hours converts it to the turbostratic phase. X-ray powder data are in accord with those in the literature for turbostratic BN (*1*), with increased resolution of the [002] reflection at 3.56 Å and the appearance of a broad peak corresponding to the [10] reflection (unresolved [100] and [101] reflections for hexagonal BN) at 2.13 Å.

Density measurements performed on the BN after the 1100°C heating step give a value of 1.7 g/cm^3, in reasonable accord with previously published data (*5*). The infrared spectrum of the turbostratic product is in agreement with published data (Fig. 1) (*6*). Electron energy loss spectroscopy (EELS) (*4*) reveals a B:N ratio of 1.00:1.06 (48.4 ± 0.3% to 51.6 ± 0.8%

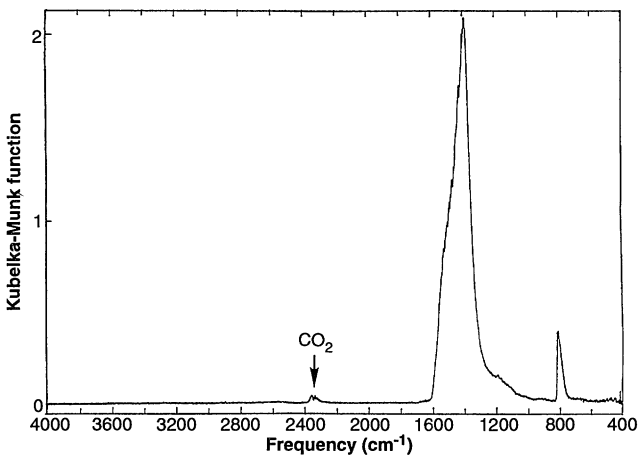

Fig. 1. Diffuse reflectance infrared spectrum of turbostratic BN.

atomic concentration). This technique has previously been used successfully for microanalysis of BN (*7*). Additionally, no residual chlorine could be detected by EELS on the material heated to 1100°C. Conventional elemental analysis also supports the BN formulation.

The SEM images of BN converted to the turbostratic form reveal, in addition to some residual amorphous material, two distinct coexisting morphologies. The first, distorted lamellar crystallites, is consistent with the partially ordered turbostratic form of BN. The second type of BN (Fig. 2) consists of hollow tubular structures, the largest of which are ~3 μm in diameter, with a typical length of 50 to 100 μm. The walls of the larger tubes have a thickness of up to 1000 Å. It is of considerable interest that the tubes appear to be aligned in a parallel orientation (Fig. 2A), and most have at least one closed, rounded end. It is possible that the other tubes lost their caps as a result of fracture (Fig. 2B).

This tubular morphology is, to our knowledge, hitherto unknown for BN. Recent reports have described needlelike graphitic carbon structures (*8*) and concentric, "onionlike" fullerene species (*9*). However, these graphitic structures have much greater internal order and are two orders of magnitude smaller than the structures we describe here. Although filaments, tubes, and shells of similar structure to tubular BN have been observed for carbon (*10*), these were formed as a result of decomposition of gases on supported metal (predominantly Ni) catalyst particles. Electron microscopy reveals the presence of metal or metal oxide particles at the ends of or filling the carbon structures. In the case of BN presented here, however, no such catalysts were used.

Energy-dispersive x-ray analysis (EDS) was performed on each of the distinct regions of the sample (*4*) (residual amorphous material, lamellar turbostratic material, and tubular turbostratic material). In each case both B and N were detected. Although for such light elements accurate atomic ratios were not obtainable, relative peak areas for B and N were invariant within experimental limitations between regions of differing morphology, confirming a homogeneous chemical composition for the sample. A small peak corresponding to oxygen was also observed, which was probably due to adsorbed oxygen, as similar amounts were seen both on the surface of the sample and on the carbon-painted stub on which the BN grains were mounted. No residual Cl or Cs was detected.

Transmission electron microscopy (TEM) of the turbostratic material (tubular and lamellar) revealed several features (*4*). Selected-area electron diffraction (ED) from a single tube wall of ~300 Å thick further indicates that the tubular BN is also turbostratic. The diffraction rings for all morphologies correspond closely to the x-ray diffraction pattern (XRD) of turbostratic BN and can be indexed by reference to the XRD pattern of hexagonal BN (*1*). The highlighted circle in Fig. 3A shows the region from which the diffraction pattern (Fig. 3B) was obtained (*11*).

A high-resolution TEM micrograph obtained from a single tube wall (Fig. 4A) clearly showed pseudographitic stacking. The observed interlayer spacing is ~3.5 Å. However, only local order exists within the wall. Boundaries are readily observable between grains of ~20 Å on edge, and the grains adopt an apparently random orientation with respect to one another. Although this is entirely consistent with the ED pattern obtained, it offers no information as to the reasons for adoption of the tubular morphology.

The TEM images also reveal the presence of smaller tubular structures with a typical diameter of 0.15 μm. In close proximity to these, there have also been observed flatter, "corpuscular" structures of similar diameter (Fig. 4B). It is possible that these corpuscles are the sites of incipient growth of the hollow fibers. The preferred parallel orientations of groups of fibers observed by SEM may be a result of their growth from a "field" of these structures attached to a relatively flat surface (Fig. 4B). These corpuscular seeds may themselves be formed from small shell-like

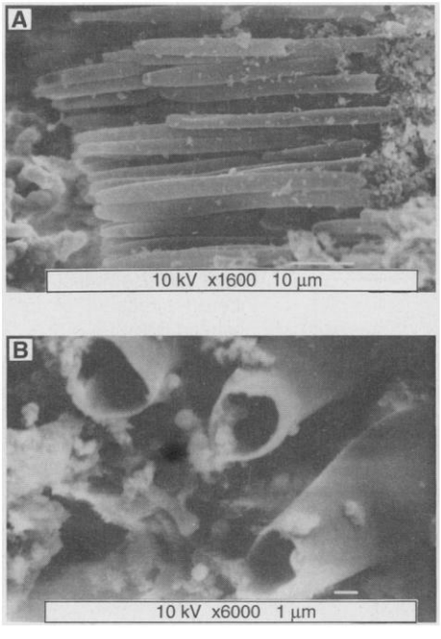

Fig. 2. (**A**) Scanning electron micrograph of a typical group of tubular BN structures and (**B**) close-up view of tube openings.

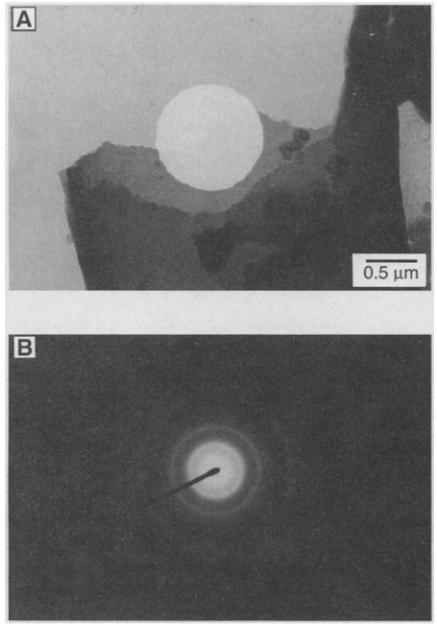

Fig. 3. (**A**) Transmission electron micrograph of BN tube fragment. Highlighted area shows region from which electron diffraction pattern (**B**) was obtained. Rings correspond to diffraction by [002], [10], [004], and [110] planes.

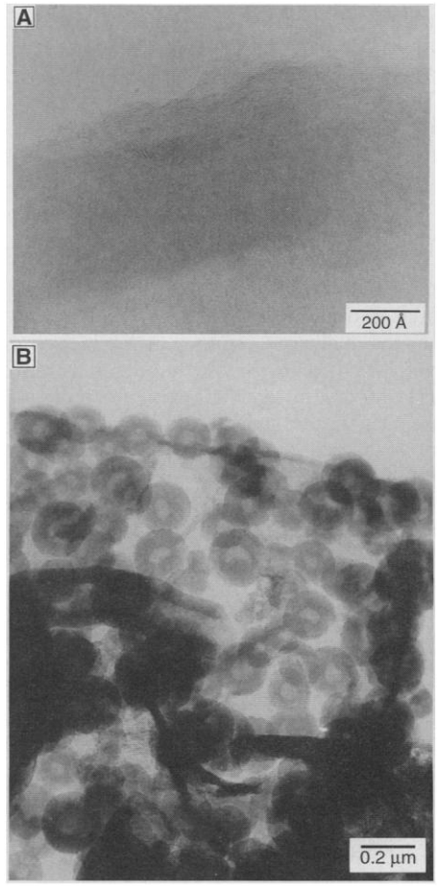

Fig. 4. (**A**) High-resolution TEM from a region of a single tube wall. Interlayer spacing is ~3.5 Å. (**B**) Transmission electron micrograph of BN corpuscles.

structures observed by TEM in the amorphous BN obtained by our synthesis.

Although these apparent sites of fiber growth have been identified, little is yet known about the exact mechanism by which the tube growth occurs or the driving forces involved. Although it is difficult to propose a mechanism for the formation of the tubes from the amorphous material, it would appear that their consistently parallel orientation is a result of conditions existing during their growth.

To our knowledge, hollow BN fibers of this type have not been reported previously. Although small, poorly crystalline BN fibrils of approximate dimensions 1 μm by 5 μm have been obtained by high-pressure pyrolysis of borazine (*12*), no indication was given of their internal structure.

REFERENCES AND NOTES

1. J. Thomas, N. W. Weston, T. E. O'Connor, *J. Am. Chem. Soc.* **84**, 4619 (1963).
2. R. T. Paine and C. K. Narula, *Chem. Rev.* **90**, 73 (1990).
3. In a typical trial in an evacuated heavy-walled glass bomb, *B*-trichloroborazine (1.72 g, 9.36 mmol) and metallic cesium (0.99 g, 7.45 mmol) reacted to produce BN [0.25 g, 55% yield based on consumed $(BClNH)_3$]. **The reactants must be loaded into the bomb in an inert atmosphere dry-box because of the extremely high reactivity of cesium.** Liberated HCl and H_2 were pumped away, unreacted *B*-trichloroborazine was removed by vacuum sublimation, and the CsCl by-product was removed by washing with water.
4. Diffuse reflectance infrared spectra (IR) were recorded with a Mattson Polaris Fourier transform IR spectrometer equipped with diffuse reflectance apparatus. X-ray powder patterns were obtained on a Rigaku Geigerflex powder diffractometer with a Cu target. Scanning electron microscopy was carried out with a JEOL 840 SEM. Energy-dispersive x-ray analysis was performed with a JEOL 820 SEM and a Link Analytical Oxford Instruments eXL EDS. Transmission electron microscopy was generally performed on a JEOL 200CX TEM, with high-resolution TEM and EELS being done on a JEOL 2010 TEM and a Gatan 666 PEELS, respectively.
5. P. J. Fazen, J. S. Beck, A. T. Lynch, E. E. Remsen, L. G. Sneddon, *Chem. Mater.* **2**, 96 (1990).
6. F. A. Miller and C. H. Wilkins, *Anal. Chem.* **24**, 1253 (1952); E. G. Brame, Jr., J. L. Margrave, V. W. Meloche, *J. Inorg. Nucl. Chem.* **5**, 48 (1957).
7. Y. Matsui, Y. Sekikawa, T. Ishii, S. Isakosawa, K. Shii, *J. Mater. Sci.* **16**, 1114 (1981).
8. S. Iijima, *Nature* **354**, 56 (1991).
9. D. Ugarte, *ibid.* **359**, 707 (1992).
10. See, for example, D. J. Smith, M. R. McCartney, E. Tracz, T. Borowiecki, *Ultramicroscopy* **34**, 54 (1990); I. Alstrup, *J. Catal.* **109**, 241 (1988), and references therein.
11. It should also be noted that a similar ED pattern was obtained from the material prior to the 1100°C heating step, which was shown to be amorphous to x-rays. This result might be explained by the presence of some more ordered areas within the essentially amorphous sample. The coexistence of crystalline and amorphous domains in fabricated BN fibers has been shown previously by ED; see D. A. Lindquist, J. F. Janik, A. K. Datye, R. T. Paine, J. B. Rothman, *Chem. Mater.* **4**, 17 (1992).
12. S.-I. Hirano, T. Yogo, S. Asada, S. Naka, *J. Am. Ceram. Soc.* **72**, 66 (1989).

13. We thank the Army Research Office for support of this work through grant DAAL03-92-G-0199. Energy-dispersive x-ray analyses were obtained by J. Mitchell of the Department of Geological Sciences of Ohio State University.

1 February 1993; accepted 25 March 1993

Banded Surface Flow Maintained by Convection in a Model of the Rapidly Rotating Giant Planets

Zi-Ping Sun, Gerald Schubert,* Gary A. Glatzmaier

In three-dimensional numerical simulations of a rapidly rotating Boussinesq fluid shell, thermally driven convection in the form of columns parallel to the rotation axis generates an alternately directed mean zonal flow with a cylindrical structure. The mean structure at the outer spherical surface consists of a broad eastward flow at the equator and alternating bands of westward and eastward flows at higher latitudes in both hemispheres. The banded structure persists even though the underlying convective motions are time-dependent. These results, although still far from the actual motions seen on Jupiter and Saturn, provide support for theoretical suggestions that thermal convection can account for the remarkable banded flow structures on these planets.

The differential rotation on the surface of the sun is characterized by one broad eastward jet in the equatorial region with high-latitude subrotation relative to the basic rotation rate (*1*, *2*). The surface differential rotation patterns on Jupiter and Saturn consist of a strong eastward jet in the equatorial region with weaker alternating westward and eastward jets extending up to 80° latitude in each hemisphere (*3*, *4*). The latitudinal structure and amplitude of Jupiter's banded zonal surface flow remained essentially constant in time during the 4 months between the Voyager 1 and Voyager 2 encounters (*3*).

Busse (*5*) introduced an analytical model showing how thermal convection in a deep rapidly rotating spherical shell might maintain a mean zonal flow and applied the model to the sun, Jupiter, and Saturn (*6*). Busse hypothesized cylindrically layered convective columnar structures aligned parallel to the axis of planetary rotation, with each convective column drifting longitudinally with constant angular velocity as part of an ordered multilayered configuration. There have been many attempts to simulate numerically the highly nonlinear convective motions and differential rotation in these internally heated rotating fluid bodies (*7*–*11*). A differential rotation in the form of an equatorial acceleration similar to that observed on the solar surface has been simulated with three-dimensional models of deep convection in a rotating spherical shell (*7*–*10*). Large eddy diffusivities were used to mimic the subgrid-scale transport of heat and momentum. In these computations, the convergence of angular momentum flux in the equatorial region maintains the differential rotation, but the angular velocity in the interior is predicted to increase with cylindrical radius and to be constant on coaxial cylinders, in contrast to the pattern inferred from helioseismology where angular velocity is constant on spheres (*4*).

One cannot invoke such large eddy diffusivities for Jupiter or Saturn because the small luminosities (internally generated heat fluxes) of these giant planets produce buoyancy forces too weak to overcome the stabilization of large viscous and thermal diffusivities. Small eddy diffusivities lead to small spatial velocity scales, which are ultimately responsible for the banded differential rotation seen on the giant planets. It is the combination of small luminosity and rapid rotation that makes numerical simulation of the giant planets so challenging. A banded differential rotation pattern similar to what is observed has been simulated by modeling Jupiter's shallow gaseous weather layer with a one-level quasi-barotropic model and a two-level quasi-geostrophic model (*11*). However, these shallow layer models neglect the internal heat flux, which is known to be important for the dynamics (*3*), ignore any influence from the vast convecting liquid interior below, and assume that the differential rotation is maintained only by two-dimensional turbulence and baroclinic instabilities in the surface layer.

According to Busse (*6*), a multilayered structure of columnar convection along cylindrical surfaces parallel to the axis of rotation will generate banded east-west surface flow by the convergence of angular

Z.-P. Sun, Department of Atmospheric Sciences, University of California, Los Angeles, CA 90024.
G. Schubert, Department of Earth and Space Sciences and the Institute of Geophysics and Planetary Physics, University of California, Los Angeles, CA 90024.
G. A. Glatzmaier, Earth and Environmental Sciences Division and the Institute of Geophysics and Planetary Physics, Los Alamos National Laboratory, Los Alamos, NM 87545.

*To whom correspondence should be addressed.